Konrad-Zuse-Zentrum für Informationstechnik Berlin

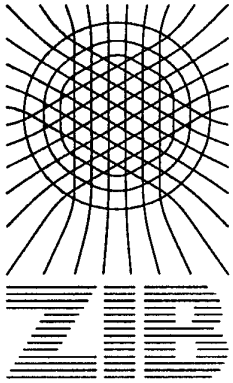

Jens Lang Artur Walter

An Adaptive Discontinuous Finite Element Method for the Transport Equation

Preprint SC 91–7 (July 1991)

An Adaptive Discontinuous Finite Element Method for the Transport Equation

Jens Lang and Artur Walter *

Abstract. In this paper we introduce a discontinuous finite element method. In our approach, it is possible to combine the advantages of finite element and finite difference methods. The main ingredients are numerical flux approximation and local orthogonal basis functions. The scheme is defined on arbitrary triangulations and can be easily extended to nonlinear problems. Two different error indicators are derived. Especially the second one is closely connected to our approach and able to handle arbitrary variing flow directions. Numerical results are given for boundary value problems in two dimensions. They demonstrate the performance of the scheme, combined with the two error indicators.

Key words. neutron transport equation, discontinuous finite element, adaptive grid refinement.

AMS(MOS) subject classifications. 65N30, 65M15.

1. Introduction

The tranport equation arises in many areas of physics, such as reactor analysis, induction of electrons in solids and the propagation of photons in stellar and planetary atmospheres. All this applications lead to equations of the form

$$\begin{aligned} \beta \cdot \nabla u(x,\beta) + \sigma(x)u(x,\beta) &= \int_{S^2} \alpha(x,\beta,\eta)u(x,\eta)d\eta + f(x,\beta) \quad \text{for } x \in \Omega \\ u(x,\beta) &= 0 \quad \text{for } x \in \Gamma_- \end{aligned} \tag{1.1}$$

where α is the transfer kernel describing the distribution of particles arising from scattering, fission and capturing events and σ is the total cross–section. Further, Ω is in general a domain in $\mathbb{R}^3$ and $\Gamma_- := \{x \in \partial\Omega : \beta \cdot n(x) < 0\}$ its inflow boundary, with $n(x)$ denoting the outer unit normal to Ω at x . The unknown function $u = u(x,\beta)$

*Konrad Zuse Zentrum für Informationstechnik Berlin Heilbronner Str. 10, D-1000 Berlin 31
Email: walter@sc.zib-berlin.dpb.de

is the density of particles, moving in the direction β.
The numerical approach in general, is to approximate the integral in (1.1) by a sum, using an angular quadrature scheme with N evaluation points, and so we have to solve N transport equations as introduced in section 2. Therefor, one should use an adaptive high resolution scheme for solving the transport equation to obtain a fast and accurate algorithm. This demands can be satisfied by a discontinuous finite element method, DFEM. This method is based on a local approach, since the solution is allowed to be discontinuous across interelement boundaries. The DFEM is already widely used for equations of the form (1.1). It was first analyzed by LESAINT & RAVIART, [8] , and more recently by JOHNSON & PITKÄRANTA , [7] , who obtained improved estimates. Later, RICHTER , [11] , developed a new approach to DFEM by using two types of triangles in his analysis. In a note on convergence PETERSON , [9] , proved optimality of this estimates for quasi–uniform meshes. Our work was stimulated by the paper of COCKBURN & SHU, [3] , in which ideas of nonoscillating finite difference methods in combination with finite element methods are used.
In the following, we will describe a variant of DFEM which can involve this ideas while keeping nice features of finite element methods, such as easy handling of complex geometries and boundary conditions. We can increase the accuracy locally rather than to use wider stencils as in finite difference methods. Another important aspect is, that within this approach it is possible to transmit the well established finite difference methodology for this equations to irregular grids and higher dimensions. The method is explicit and able to work on very irregular grids. This is necessary , since during the solution process the grid will be adapted to the solution.
Two error indicators are derived and compared. The first uses a dual problem in a standard way. The second is based on the ease of increasing *locally* the degree of the approximating polynomials in the context of DFEM. For this, we choose a basis of orthogonal polynomials on each triangle. So, we can split the solution in it's constant and linear part. The magnitude of the linear part is taken as an error indicator. This different motivation are reflected in a quite different behavior of the indicators in our applications.
The outline of the paper is as follows. In the second section we introduce the model equation and our scheme. It is shown, that it fitts between finite difference and finite element methods. In the third section an error estimation is given for the case of a constant flow field vector β. For an abitrary vector β we introduce the idea of local orthogonal basis functions and the corresponding error indicator. The last section includes some numerical experiments merely done to show the performance of the different indicators. Finally, a conclusion and some remarks on the discretization of convection–diffusion equations are given.

2. Scalar linear transport equation and discretization

We consider the first–order hyperbolic equation

$$\begin{aligned} \beta \cdot \nabla u + \sigma u &= f \quad \text{in} \quad \Omega \,, \\ u &= g \quad \text{on} \quad \Gamma_- \,. \end{aligned} \tag{2.1}$$

as a model of equation (1.1). Here, Ω is a bounded polygonal domain in $\mathbb{R}^2$. The flow field vector $\beta : \Omega \to \mathbb{R}^2$ is a prescribed smooth vector field, and σ is a bounded measurable function on Ω and g the given inflow condition.

For a finite element triangulation $T_h = \{T\}$ of Ω, we denote by $P_\kappa(T)$ the space of polynomials of degree $\leq \kappa$ on $T \in T_h$. The DFEM for (2.1) is derived from the weak formulation on each $T \in T_h$. We replace the exact solution u by its possible discontinuous approximation u_h with $u_h|_T \in P_\kappa(T)$. Finally, integrating by parts yields for $v_h|_T \in P_\kappa(T)$

$$\int_T u_h(-\nabla \cdot (\beta v_h) + \sigma v_h)dx + \int_{\partial T} u_h v_h \beta \cdot n \; ds = \int_T f v_h dx \,. \tag{2.2}$$

Since u_h is piecewise polynomial of degree κ over the triangulation T it is not exactly defined at ∂T. This gives many possibilities to choose this variables at the boundaries. In the following we will use this to adopt the successful nonoscillatory methodology , see e.g. [6], from the finite difference method. We replace the flux function $u_h \beta \cdot n$ by some numerical average flux $h(u_h^{\text{int}}, u_h^{\text{ext}})$. With the definitions for a $x \in \partial T$

$$\begin{aligned} u_h^{\text{int}} &:= \lim_{x^i \to x} u_h(x^i) \quad \text{for } x^i \in \text{interior of T} \\ u_h^{\text{ext}} &:= \lim_{x^i \to x} u_h(x^i) \quad \text{for } x^i \in \text{exterior of T} \end{aligned}$$

we can use e.g. a Lipschitz continuous "monotone" flux as given in [3]. Such a function $h(\cdot,\cdot)$ satisfies the consistency relation $h(u,u) = u\beta \cdot n$, is nondecreasing in its first argument and nonincreasing in its second argument. Scheme (2.2) now reads:

Find $u_h|_T \in P_\kappa(T)$ such that for each triangle $T \in T_h$

$$\int_T u_h(-\nabla \cdot (\beta v_h) + \sigma v_h)dx + \int_{\partial T} h(u_h^{\text{int}}, u_h^{\text{ext}}) v_h ds = \int_T f v_h dx \,, \; \forall v_h \in P_\kappa(T) \,. \tag{2.3}$$

A possible choice of $h(\cdot,\cdot)$ is the Engquists–Osher two–point monotone flux, which for an arbitrary function $fl(u)$ is defined as

$$h^{EO}(a,b) = \int_0^b \min(fl'(s),0)ds + \int_0^a \max(fl'(s),0)ds + fl(0)\,. \tag{2.4}$$

Now, the following result gives an interesting connection to the usually discontinuous Galerkin method introduced by REED & HILL [10]. First we recall their formulation of the method: Seek a function $u_h|_T \in P_\kappa(T)$ such that for all $T \in T_h$

$$\int_T (\beta\cdot\nabla u_h + \sigma u_h)v_h dx + \int_{\partial T_-} (u_h^+ - u_h^-)v_h|\beta\cdot n|ds = \int_T f v_h dx\,,\ \forall v_h \in P_\kappa(T)\,, \tag{2.5}$$

with $\partial T_- = \{x \in \partial T : \beta\cdot n(x) < 0\}$ and $u_h^\pm = \lim_{\varepsilon\to 0^\pm} u_h(x+\varepsilon\beta)$.

Lemma 2.1 *The method* (2.5) *is equivalent to* (2.3) *with the numerical flux approximation* (2.4).

Proof. For $fl(u) = u\beta\cdot n$ we get with (2.4)

$$\begin{aligned}\int_{\partial T} h^{EO}(u_h^{\text{int}}, u_h^{\text{ext}})v_h ds &= \int_{\partial T}(u_h^{\text{ext}}\min(\beta\cdot n,0) + u_h^{\text{int}}\max(\beta\cdot n,0))v_h ds\\ &= \int_{\partial T_+} u_h^{\text{int}} v_h|\beta\cdot n|ds - \int_{\partial T_-} u_h^{\text{ext}} v_h|\beta\cdot n|ds\,,\end{aligned}$$

with $\partial T_+ = \{x \in \partial T : \beta\cdot n(x) \geq 0\}$. The reformulations

$$u_h^{\text{int}}|_{\partial T_+} = u_h^- \quad,\quad u_h^{\text{ext}}|_{\partial T_-} = u_h^-$$

yield for the left–hand side of (2.3) after integrating by parts the equality

$$\begin{aligned}&\int_T u_h(-\nabla\cdot(\beta v_h) + \sigma v_h)dx + \int_{\partial T} h^{EO}(u_h^{\text{int}}, u_h^{\text{ext}})v_h ds\\ &\quad= \int_T(\beta\cdot\nabla u_h + \sigma u_h)v_h dx - \int_{\partial T_+} u_h^- v_h|\beta\cdot n|ds + \int_{\partial T_-} u_h^+ v_h|\beta\cdot n|ds +\\ &\qquad+ \int_{\partial T_+} u_h^- v_h|\beta\cdot n|ds - \int_{\partial T_-} u_h^- v_h|\beta\cdot n|ds\\ &\quad= \int_T(\beta\cdot\nabla u_h + \sigma u_h)v_h dx + \int_{\partial T_-}(u_h^+ - u_h^-)v_h|\beta\cdot n|ds\end{aligned}$$

which proves the lemma. ∎

Remark 2.2 Therefor, with the above Lemma 2.1 the usual discontinuous Galerkin method, as analyzed in [7], is a special case of the generalized discontinuous Galerkin method (2.3). This fact gives us a hint how to handle the more complicate problem of a nonlinear flow field vector, as e.g. in Burgers equation $\beta := u \cdot \nabla u$. A second important aspect of this approach is it's ability to transmit the well established finite difference schemes to very irregular grids.

It has been shown in [8] that for constant β an ordering of the triangles $\{T_1, T_2, \ldots\}$ exists such that the finite element approximation can be computed in an explicit way. The same was done in [5] if $|\beta \cdot n| > 0$ for all sides of triangles in T_h. The ordering is also possible if $div(\beta) = 0$, see [13]. For this cases, transport problems like (2.1) seem connected to explicit methods in a natural way.

For further analysis, we introduce for each triangle T a finite element space V_h defined by

$$V_h := \{v_h \in L_2(\Omega) : v_h|_T \in P_\kappa(T)\,,\ T \in T_h\}\ .$$

Note, that any choice of the degrees of freedom of the approximate solution is allowed in this formulation, c.f. [5]. Summing up over all $T \in T_h$ in (2.3), we arrive at the following equivalent formulation of (2.3) : Find $u_h \in V_h$ such that

$$B(u_h, v_h) = (f, v_h)\,,\ \forall v_h \in V_h \tag{2.6}$$

where

$$B(w, v) := \sum_{T \in T_h} \{(w, -\nabla \cdot (\beta v) + \sigma v)_T + (h, v)_{\partial T}\}\ . \tag{2.7}$$

Here $(\cdot,\cdot)_T$, $(\cdot,\cdot)_{\partial T}$ denote the $L_2(T)$, $L_2(\partial T)$ inner products. Of course, we can replace u_h by the exact solution u in (2.6), i.e., we have the consistency relation

$$B(u - u_h, v_h) = 0 \quad v_h \in V_h\ . \tag{2.8}$$

3. Error Estimates

3.1 Constant unit flow field vector β

For constant unit β JOHNSON & PITKÄRANTA [7] obtained for the usual discontinuous Galerkin method (2.5) various stability and convergence results, including an L_2–error estimate of the form

$$\|u - u_h\|_{0,\Omega} \leq C \cdot h^{\kappa+\frac{1}{2}} |u|_{\kappa+1,\Omega} \,. \tag{3.1}$$

This error estimate is based on a stability inequality

$$|u_h|_{h,\beta} + \|u_h\|_{0,\Omega} \leq C \left(\|f\|_{0,\Omega} + \|g\|_{0,\Gamma_-} \right) , \tag{3.2}$$

where $|\cdot|_{h,\beta}$ is a mesh–dependent seminorm which controls the derivative $\beta \cdot \nabla u_h$ and the jumps of $u_h \beta \cdot n$ across the interelement boundaries. This stability result is, of course, also true for (2.3),(2.4). In what follows, we will present another proof of the convergence result (3.1) using only a special part of $|\cdot|_{h,\beta}$,

$$\|(u_h^+ - u_h^-)|\beta \cdot n|^{1/2}\|_{0,\Gamma_h} \leq |u_h|_{h,\beta} \,. \tag{3.3}$$

All interelement boundaries are denoted by $\Gamma_h := \left(\bigcup_{T \in T_h} \partial T \right) \setminus \partial\Omega$.

We start our derivation by considering the dual problem to (2.1) for $\Theta \in L_1(\Omega)$:

$$\begin{aligned} -\beta \cdot \nabla \varphi + \sigma \varphi &= \Theta \text{ in } \Omega \,, \\ \varphi &= 0 \text{ on } \Gamma_+ \,. \end{aligned} \tag{3.4}$$

In the next step we seek an approximate solution $\varphi_h \in V_h$ such that

$$B(v_h, \varphi_h) = (\Theta, v_h) \,, \; v_h \in V_h \tag{3.5}$$

where B is as in (2.7), with $h = h^{EO}$. Setting $w = v_h$ and $v = \varphi_h$ in (2.7), we get

$$\sum_{T \in T_h} (h^{EO}, \varphi_h) = \int_{\Gamma_h} v_h^- (\varphi_h^- - \varphi_h^+) |\beta \cdot n| ds \,.$$

Here, for a piecewise continuous function v_h we define $v_h^-(x) = \lim_{\varepsilon \to 0^-} v(x - \varepsilon\beta)$, $x \in \Gamma_h$. The function φ_h is the solution to the problem (3.4). Now, we introduce the local L_2–projection $\tilde{u} \in V_h$ of the exact solution u by

$$\int_T (u - \tilde{u}) v \, dx = 0 \,, \; v \in P_\kappa(T) \,, \; T \in T_h \,.$$

Applying the Bramble–Hilbert lemma [2] and a standard estimate of norms over boundaries, see e.g. [1], we get

$$\begin{aligned} \|u - \tilde{u}\|_{0,T} &\leq C h^{\kappa+1} |u|_{\kappa+1,T} \,, \\ \|u - \tilde{u}\|_{0,\partial T} &\leq C h^{\kappa+1/2} |u|_{\kappa+1,T} \,. \end{aligned}$$

With the choice $\Theta = v_h = (u_h - \tilde{u}) \in V_h$ and recalling (2.8), it is

$$\|u_h - \tilde{u}\|^2_{0,\Omega} = B(u - \tilde{u}, \varphi_h) = (u - \tilde{u}, -\beta \cdot \nabla\varphi_h + \sigma\varphi_h) + \int_{\Gamma_h} (u - \tilde{u})^-(\varphi_h^- - \varphi_h^+)|\beta \cdot n| ds \, .$$

Since $\beta \cdot \nabla\varphi_h \in V_h$ and with (3.2), (3.3), it follows by Cauchy–Schwarz inequality that

$$\|u_h - \tilde{u}\|_{0,\Omega} \leq (C_1 \, h^{\kappa+1/2} + C_2\|\sigma\|_{\infty,\Omega} h^{\kappa+1})|u|_{\kappa+1,\Omega} \, .$$

Using the triangle inequality we finally obtain

$$\begin{aligned} \|u - u_h\|_{0,\Omega} &\leq \|u - \tilde{u}\|_{0,\Omega} + \|u_h - \tilde{u}\|_{0,\Omega} \\ &= \left(C_1 h^{\kappa+1/2} + C_2(\|\sigma\|_{\infty,\Omega} + 1) h^{\kappa+1}\right) |u|_{\kappa+1,\Omega} \, . \end{aligned} \tag{3.6}$$

This completes the proof. ∎

An obvious idea to improve u_h during an adaptive process is the equidistribution of all local element errors. To give (3.6) a practical meaning, an approximation $D_T^{\kappa+1} u_h$ of the Sobolev seminorm $|u|_{\kappa+1,T}$ is needed. This can be done by using the numerical solution u_h. We refer the interested reader to [4].
For a local error indicator we can use

$$\|u - u_h\|_{0,T} \approx C(h^{\kappa+\frac{1}{2}} + (\|\sigma\|_{\infty,T} + 1) h^{\kappa+1}) D_T^{\kappa+1} u_h \quad , T \in T_h \tag{3.7}$$

3.2 Arbitrary flow field vector β

The situation becomes more complicate if β is an arbitrary vector function, not necessary constant or with vanishing divergence. In this case neither stability nor convergence results are known. Nevertheless, we can use the flexibility of our scheme in increasing locally the degree of the approximating polynomials. In this way, we can get an efficient error indicator, if we choose the polynomials appropriate.
For the implementation of (2.6) we use a *local orthogonal basis* in $P_\kappa(T)$, $\{v_0^T, v_1^T, \ldots, v_\ell^T\}$, $\ell \in \mathbb{N}$, such that v_i^T has support in T and

$$(v_i^T, v_j^T) = C_i \delta_{ij} \, , \; C_i \neq 0 \, , \; i, j = 0, 1, \ldots, \ell \, .$$

This orthogonality is achieved by choosing an orthogonal basis over the standard triangle $\triangle := \{(\xi, \eta) \in \mathbb{R}^2 : 0 \leq \xi, \eta \leq 1, \xi + \eta \leq 1\}$

$$v_0^\triangle = 2, \; v_1^\triangle = 6\xi - 2, \; v_2^\triangle = 2\sqrt{6}(\xi + 2\eta - 1), \; \ldots \, .$$

For simplicity of presentation, we restrict ourselves to the case $\kappa = 1$, i.e. linear polynomials. Using an affine–linear mapping $F : \Delta \to T \in T_h$, we get in this case,

$$\begin{aligned} v_0^T &= \tfrac{1}{2} v_0^{\Delta}(\xi(x_1,x_2),\eta(x_1,x_2) = 1 \,, \\ v_i^T &= \sqrt{\tfrac{|T|}{2}} v_i^{\Delta}(\xi(x_1,x_2),\eta(x_1,x_2)),\ i = 1,2 \,, \end{aligned} \tag{3.8}$$

where $|T|$ stands for the area of T. The choice of the constants will become clear below. If we define the degrees of freedom as

$$u_T^{(m)} = \frac{1}{|T|^{\gamma}} \int_T u v_m^T dx \,,\ T \in T_h \,,\ m = 0,1,2 \ , \tag{3.9}$$

with $\gamma = 1$ if $m = 0$ and $\gamma = 2$ if $m = 1,2$, we get the approximation of the exact solution in V_h by

$$u_h(x) = \sum_{m=0}^{2} u_T^{(m)} v_m^T(x) \,,\ x \in T \,,\ T \in T_h \,. \tag{3.10}$$

Clearly, the process described above is applicable for arbitrary $\ell \in \mathbb{N}$, too. We mention, that $u_T^{(0)}$ is an approximation of the average of the exact solution u in T. Moreover, by our construction (3.8), the basic function v_i^T, $i = 1,2$, vanishes in the midpoint x^{mid} of the triangle T, i.e., for $\kappa = 1$

$$u_h(x^{\mathrm{mid}}) = u_T^{(0)} \,. \tag{3.11}$$

Hence, we can concentrate the degrees of freedom (3.8) as cell variables in the midpoint of all $T \in T_h$. We are now working over the dual triangulation in a natural way.

Considering $u_T^{(0)}$ as an improved local numerical solution with piecewise constant trial functions (this is not the same as for $\kappa = 0$!), we can use for arbitrary κ the local error estimate

$$\|u - u_h\|_{0,T} \approx \|u_T^{(0)} - u_h\|_{0,T} = \| \sum_{m=0}^{2} u_T^{(m)} v_m^T(x) \| \ ,\ T \in T_h \tag{3.12}$$

in an adaptive process.

4. Numerical Results

The numerical experiments are mainly done to demonstrate the different behavior of the two error indicators (3.7) and (3.12) and the high accuracy of the method. For the first example, the tranportation of a discontinuous inflow condition along a straight line, both error indicators are applied. The behavior during the refinement process and the final grids, which are necessary to obtain the exact solution with our algorithm are compared. Our aim is to show, that the scheme is able to resolve the jump in the solution with a small number of grid points. The second example is a transportation of the inflow condition along circular lines around the origin. This problem is known in the literature as a very hard one, because the streamlines are bended and the distance between inflow and outflow boundary is relatively long. The divergence of the corresponding flow field is zero, and the triangles can be ordered to obtain an explicit algorithm.

4.1 Example 1: Transportation along a line

The first problem we consider is equation (2.1) on $\Omega = (0;1) \times (0;1)$ with $\sigma = 0$, $f = 0$ and the flow direction $\beta = (1.0; 1.0)$. The inflow boundaries are the lines $\{(x,y) \in \mathbb{R}^2 : x = 0\}$ and $\{(x,y) \in \mathbb{R}^2 : y = 0\}$ with the boundary condition

$$g(x,y) := \begin{cases} 0 & \text{if } y > \frac{1}{16} \\ 1 & \text{else} \end{cases} .$$

So, the discontinuity in the boundary condition doesn't coincide with the initial grid lines. The calculations are done on the basis of the program KASKADE implemented by [12]. It should be mentioned, that in nearly all applications published, the grid lines are posed to represent the discontinuity of $g(x,y)$ at the inflow boundary.

The first picture shows the intermediate grid, produced by the first error indicator, left, and the second indicator, right. They are applied in such a way, that at each refinement step no more than 1/4 of the coarser grid triangles are refined. It can be seen, that both indicators try to resolve the discontinuous inflow condition. The difference occurs at the outflow boundary. Through the explicit solution process, the flow field is calculated along β and the greatest amount of error is at the outflow part of $\partial\Omega$. The derivation of the first error indicator started from the adjoint problem (3.4) to (2.1), especially β is replaced by $-\beta$, the opposite flow direction. So, it takes this rough solution as a reference. This is also reflected on the solution after three refinement steps, which is shown in figure 2. The solution is plotted such that each triangle is coulored with respect to $u_T^{(0)}$. We divided the range from -1 to 2 in 16 equidistant gray scales to include possible over- and undershoots. On each grid point we have as many solution values as triangles belonging to this point. The solution is not interpolated nor smoothed to show the high resolution of the scheme.

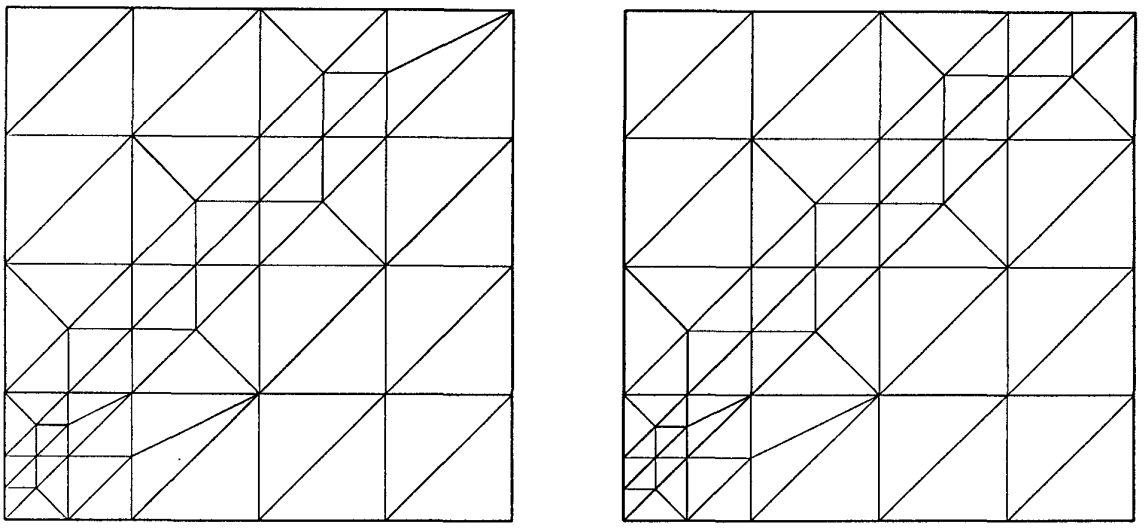

Figure 1: Intermedeate grids for example 1

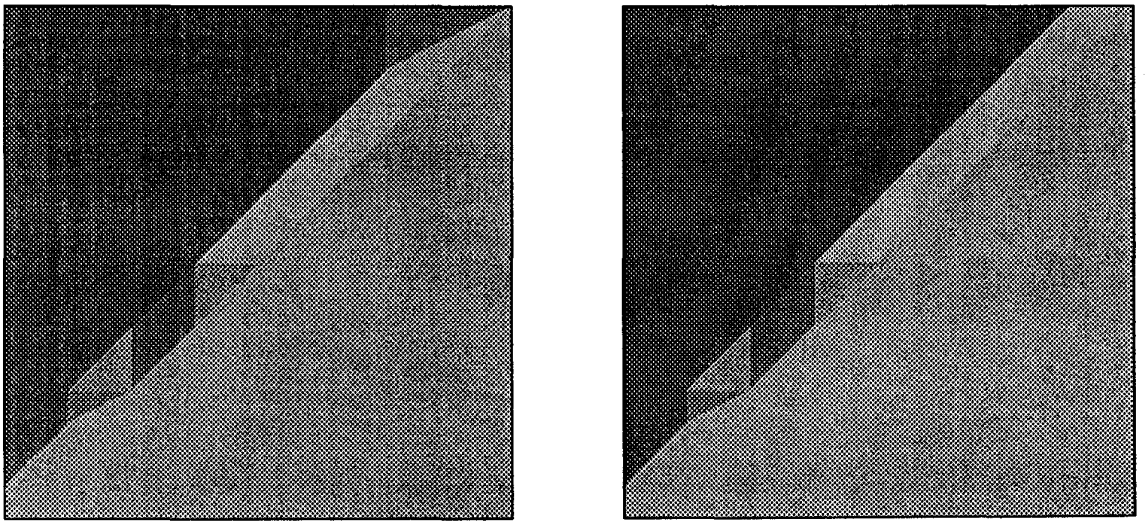

Figure 2: Solution of example 1 on intermediate grids

On the left grid, produced by indicator (3.7), the algorithmn is not able to resolve the outflow in the same manner as on the grid generated by (3.12).

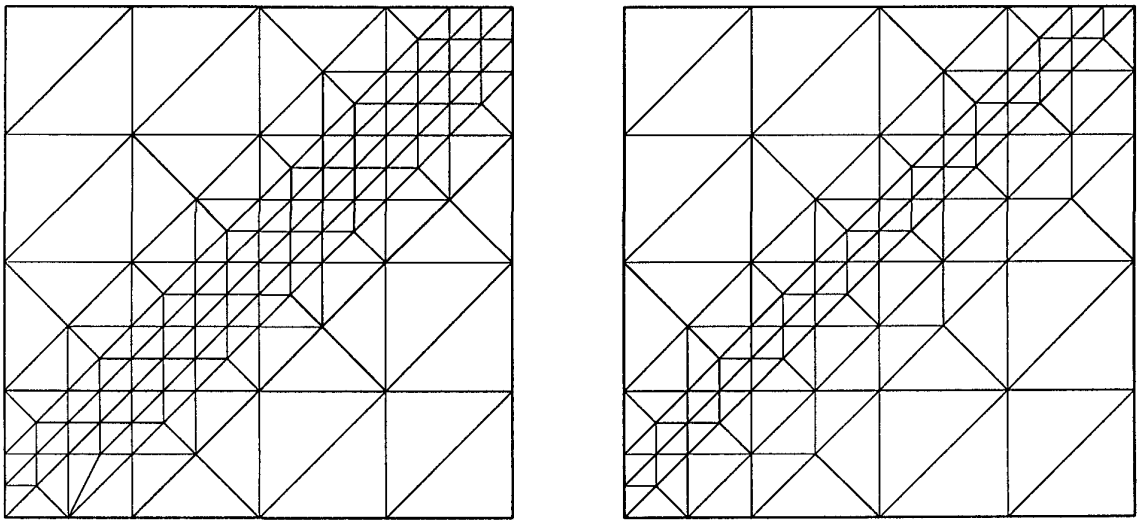

Figure 3: Final grids

In figure 3 the final grids, which were necessary to reproduce the exact solution, are shown. The left grid, corresponding to (3.7) is one refinement level deeper than the right one for the reasons discussed above.

4.2 Example 2: Rotating cone problem

In this case equation (2.1) is given on a domain $\Omega = \{(-1.0;1.0) \times (-1.0;1.0)\}\backslash\Gamma$ with the variable flow direction $\beta = (y, -x)$. It is $\sigma = 0$, $f = 0$ and the boundary condition on the inflow part set to zero with the exception of $\Gamma := \{(x;y) : x = 0 \wedge 0 \leq y \leq -1\}$. Here we use

$$g(y) := \begin{cases} 0 & \text{if } 0 \geq y > -0.1 \\ 1 & \text{if } -0.1 \geq y \geq -0.5 \\ 0 & \text{if } -0.5 > y \geq -1.0 \end{cases}$$

The exact solution is a transport of this "rectangular" inflow condition along circular lines around the origin to the outflow boundary, which is located opposite to Γ . In this case, the indicator (3.7) had had no theoretical motivation, at least in our derivation, in section 3 . So, it should be not applied here. These considerations are inforced by the numerical results.

The figure 4 shows the grid, produced by (3.12) and the solution after six refinement steps. It can be seen, that the algorithm begins to resolve the discontinuous solution starting from the inflow boundary along the streamlines.

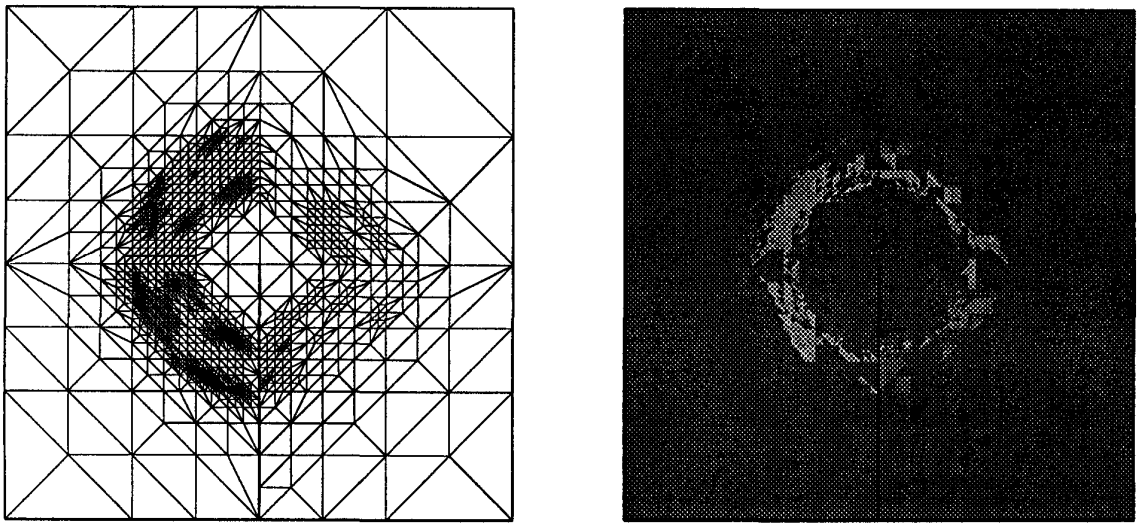

Figure 4: Intermideate grid and solution for example 2

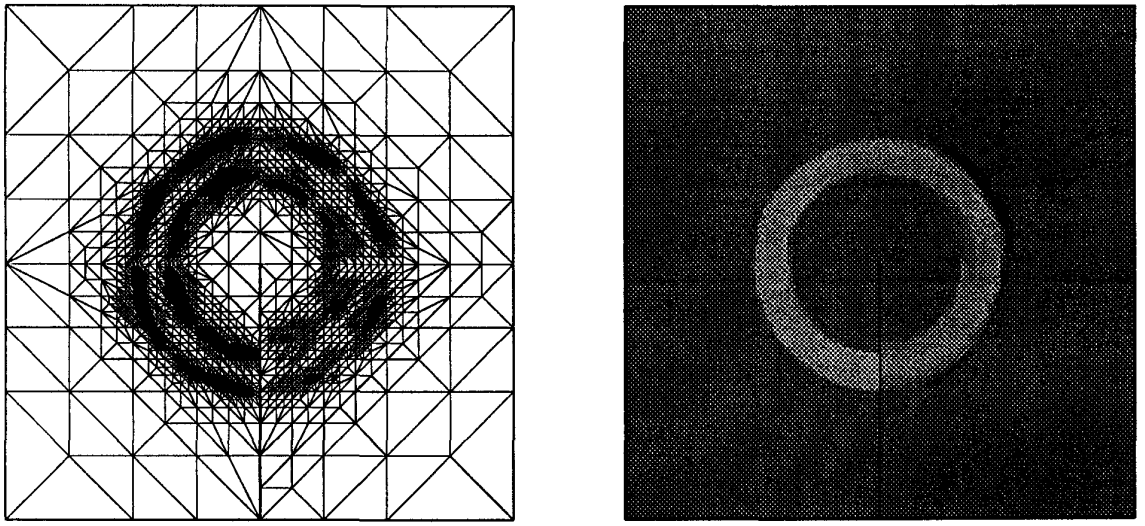

Figure 5: Final grid and solution for example 2

It is also interesting to see, that the longer the streamlines are, the more difficult it is to resolve the discontinuity.

Figure 5 shows the final grid with about 8000 triangles. The error is approximately 10% . The time lasted to obtain this solution was about 8 minutes on a Sun–Sparc–

1 workstation. To compare this result, we mention [5]. There, they need nearly 20000 triangles to follow a smooth inflow condition transported along grid lines on an equidistant grid. In spite of our remark on indicator (3.7) made above, we tried it on the same problem. The result is shown in figure 6.

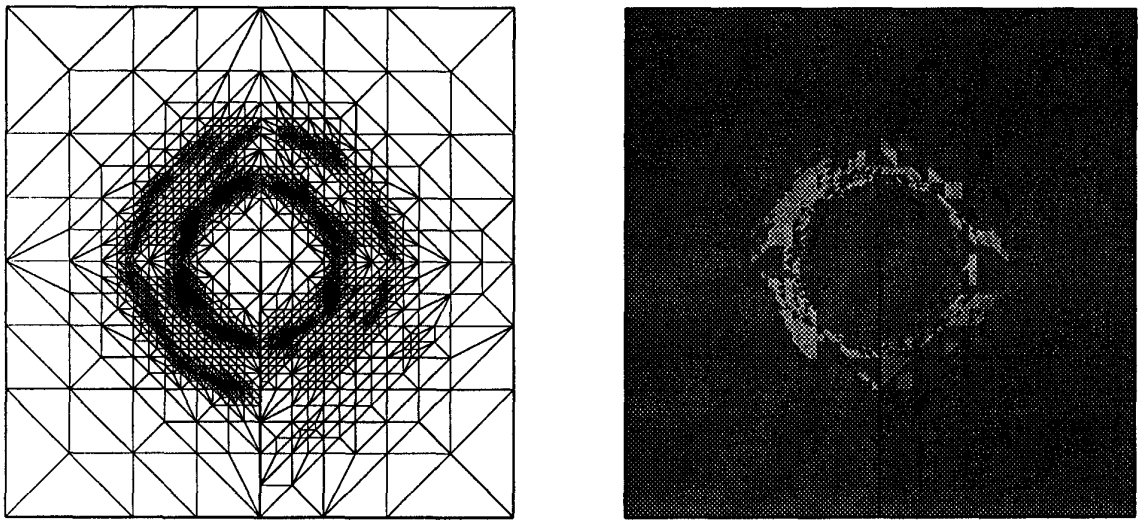

Figure 6: Grid and solution for example 2 with indicator (3.12)

The indicator was not able to transport the refined grid. After four refinement steps all further refinement takes place near the inflow region of Ω. The grid consists of more than 10000 triangles and gives an evidently worst solution than in figure 5.

5. Concluding Remarks

We have proposed a discontinuous finite element method for the transport equation. The method is of arbitrary order and can be applied in an explicit manner on quite irregular grids. Through it's derivation the scheme can combine the nice features of finite element methods with successful techniques of finite difference schemes. Furthermore, it provides a very useful and robust error indicator. Our analysis and numerical results suggest, that it can be used in a rather efficient manner in general situations.

One extension of the method should be the calculation of convection dominated convection–diffusion equations. In our approach, we approximate the solution by linear functions over each triangle. So, we have to solve 3×3 linear systems locally. Since the solution is possibly discontinuous across interelement boundaries, the Laplacian operator cannot be discretized in a suitable manner. A remedy is to split

the equation into two transport equations, as it is done in the mixed finite element method. However, this means that we have to solve 15×15 linear systems on each triangle; a significant increase in numerical work. This seems not practical to us. This topic constitutes the subject of ongoing work.

Acknowledgement The authors would like to thank R. Roitzsch for his patient support during the implementation of the algorithm.

References

[1] R. A. Adams: *Sobolev Spaces.* Academic Press New York, 1975.

[2] J. H. Bramble, S. R. Hilbert: *Estimatioan of linear functionals on Sobolev spaces with application to Fourier transforms and spline interpolation.* SIAM J. Numer. Anal., Vol. 7, pp. 112–124 (1970).

[3] B. Cockburn, C.–W. Shu: *TVB Runge–Kutta Local Projection Discontinuous Galerkin Finite Element Method for Conservation Laws II: General Framework.* Math. of Comput., Vol. 52, No. 186, pp. 411–435 (1989).

[4] K. Erikson, C. Johnson: *Adaptive Streamline Diffusion Finite Element Methods for Convection–Diffusion Problems.* Technical Report, Dept. of Methematics, Chalmers Univ. of Technology, 1990.

[5] R. S. Falk , G. R. Richter: *Analysis of a Continuous Finite Element Method for Hyperbolic Equations.* SIAM J. Num. Analy. Vol. 24, No. 2, pp. 257-278, 1987.

[6] A. Harten, S. Osher: *Uniformly High-Order Accurate Nonoscillatory Scheme I.* SIAM J. Num. Analy. Vol. 24, No. 2, pp. 279-309, 1987.

[7] C. Johnson, J. Pitkäranta: *An Analysis of the Discontinuous Galerkin Method for a Scalar Hyperbolic Equation.* Math. of Comput., Vol. 46, No. 173, pp. 1–26 (1986).

[8] P. Lesaint, P.–A. Raviart: *On a finite element method for solving the neutron transport equation.* In: (C. de Bour, ed.), Mathematical Aspects of Finite Elements in Partial Differential Equations, Academic Press, New York, pp. 89–123 (1974).

[9] T. E. Peterson: *A Note on the Convergence of the Discontinuous Galerkin Method for a Scalar Hyperbolic Equation.* SIAM J. Num. Analy. Vol. 28, No. 1, pp. 133–140 (1991).

[10] W. H. Reed, T. R. Hill: *Triangular mesh methods for the neutron transport equation.* Technical Report LA–UR–73–479, Los Alamos National Laboratory, Los Alamos, NM (1973).

[11] G. R. Richter *An Optimal Error Estimate for the Discontinuous Galerkin Method.* Math. of Comput., Vol. 50, No. 181, pp. 75–88 (1988).

[12] R. Roitzsch: *KASKADE Programmer's Manual.* Technical Report TR89–5, Konrad Zuse Zentrum für Informationstechnik Berlin, 1989.

[13] R. Touzani: *Implementation of the Discontinuous Finite Element Method for Hyperbolic Equations.* Comput. Meths. Appl. Mech. Engrg. Vol. 68, pp. 115–123 (1988)